Geophysical Journal International

Geophys. J. Int. (2023) **232,** 2160–2174
Advance Access publication 2022 July 26
GJI Seismology

https://doi.org/10.1093/gji/ggac284

The global seismographic network reveals atmospherically coupled normal modes excited by the 2022 Hunga Tonga eruption

A. T. Ringler [1,4], R. E. Anthony [1,4], R. C. Aster,[2] T. Taira [3], B. R. Shiro,[4] D. C. Wilson,[1,4] S. De Angelis,[5] C. Ebeling,[6] M. Haney [7], R. S. Matoza [8] and H. D. Ortiz [8]

[1] *U.S. Geological Survey, Albuquerque Seismological Laboratory, Albuquerque, NM 87117, USA. E-mail:aringler@usgs.gov*
[2] *Warner College of Natural Resources, Colorado State University, Fort Collins, CO 80523, USA*
[3] *Department of Earth and Planetary Science, University of California, Berkeley, CA 94720, USA*
[4] *U.S. Geological Survey, Geological Hazards Science Center, Golden, CO 80401, USA*
[5] *Department of Earth, Ocean and Ecological Sciences, University of Liverpool, Liverpool L69 3BX, United Kingdom*
[6] *Scripps Institution of Oceanography, University of California, San Diego, CA 92093, USA*
[7] *U.S. Geological Survey, Alaska Volcano Observatory, Alaska 99508, USA*
[8] *Department of Earth Science and Earth Research Institute, University of California, Santa Barbara, CA 93106, USA*

Accepted 2022 July 21. Received 2022 July 20; in original form 2022 April 4

SUMMARY

The eruption of the submarine Hunga Tonga-Hunga Ha'apai (Hunga Tonga) volcano on 15 January 2022, was one of the largest volcanic explosions recorded by modern geophysical instrumentation. The eruption was notable for the broad range of atmospheric wave phenomena it generated and for their unusual coupling with the oceans and solid Earth. The event was recorded worldwide across the Global Seismographic Network (GSN) by seismometers, microbarographs and infrasound sensors. The broad-band instrumentation in the GSN allows us to make high fidelity observations of spheroidal solid Earth normal modes from this event at frequencies near 3.7 and 4.4 mHz. Similar normal mode excitations were reported following the 1991 Pinatubo (Volcanic Explosivity Index of 6) eruption and were predicted, by theory, to arise from the excitation of mesosphere-scale acoustic modes of the atmosphere coupling with the solid Earth. Here, we compare observations for the Hunga Tonga and Pinatubo eruptions and find that both strongly excited the solid Earth normal mode ${}_0S_{29}$ (3.72 mHz). However, the mean modal amplitude was roughly 11 times larger for the 2022 Hunga Tonga eruption. Estimates of attenuation (Q) for ${}_0S_{29}$ across the GSN from temporal modal decay give $Q = 332 \pm 101$, which is higher than estimates of Q for this mode using earthquake data ($Q = 186.9 \pm 5$). Two microbarographs located at regional distances (<1000 km) to the volcano provide direct observations of the fundamental acoustic mode of the atmosphere. These pressure oscillations, first observed approximately 40 min after the onset of the eruption, are in phase with the seismic Rayleigh wave excitation and are recorded only by microbarographs in proximity (<1500 km) to the eruption. We infer that excitation of fundamental atmospheric modes occurs within a limited area close to the site of the eruption, where they excite select solid Earth fundamental spheroidal modes of similar frequencies that are globally recorded and have a higher apparent Q due to the extended duration of atmospheric oscillations.

Key words: Acoustic properties; Seismic instruments; Surface waves and free oscillations; Volcano seismology.

INTRODUCTION

The Hunga Tonga-Hunga Ha'apai (Hunga Tonga) volcanic eruption began its most energetic phase at around 04:14:00 15 January 2022, UTC and was rapidly identified as a seismic event and assigned a surface wave magnitude (M_s; 20 s period) of 5.8 (Bormann 2012) by the U.S. Geological Survey (USGS) National Earthquake Information Center (NEIC). However, earthquake magnitudes are not appropriate for scaling volcanic eruptions, and longer-period observations recorded by high signal-to-noise very broad-band (VBB) seismographic networks (e.g. Ringler *et al.* 2022) can be used to rapidly parametrize volcanic source parameters. For example, using 10–1000 s period seismic observations across the Global Seismographic (GSN), GEOFOrschungsNetz (GEOFON) and GEOSCOPE

Networks, Poli & Shapiro (2022) estimate the Hunga Tonga eruption to have a Volcano Explosivity Index (VEI) of 6, where the VEI is a semi-quantitative scale used to characterize the explosivity of eruptions (Newhall & Self 1982). The VEI scale is based on estimates of the total volume of erupted products and the maximum height reached by the eruptive plume; as such VEI estimates are challenging for eruptions with complex source mechanisms including magma–water interaction, like Hunga Tonga (Matoza *et al.* 2014; Witze 2022). Nonetheless, a VEI 6 places the Hunga Tonga eruption as the largest explosive eruption worldwide since the (significantly more temporally extended and magmatically voluminous) VEI 6 Pinatubo (Philippines) eruption of 15 June 1991 (NASA 2022).

The 1991 eruption of Pinatubo occurred shortly after the development of modern VBB force-feedback seismometers and digital systems capable of recording long-period oscillations with high fidelity (Ringler *et al.* 2022). The GSN and other such networks were in the process of being built out at this time. However, unique long-period spheroidal normal mode oscillations of the Earth were soon identified on the GSN station MAJO (Matsushiro, Japan) and at globally distributed International Deployment of Accelerometer (IDA) gravimeters (Kanamori & Mori 1992; Widmer & Zürn 1992). Unlike the multiple normal mode oscillations of the Earth generated by great earthquakes (e.g. Nishida 2013; Schneider & Deuss 2021), Pinatubo excited only two modal frequencies: a dominant oscillation at 4.44 mHz (225 s period), and a smaller amplitude oscillation at 3.68 mHz (272 s), producing a 'bi-chromatic' spectrum. Using particle motions and estimates of propagation velocities, these signals were shown to be consistent with a Rayleigh wavefield (elliptical motion in the direction of wave propagation) originating from the Pinatubo region (Kanamori & Mori 1992; Widmer & Zürn 1992).

The excitation of such low frequency, bi-chromatic Rayleigh waves and their associated normal modes is rare. Zürn & Widmer (1996) searched for similar signals following eleven other significant volcanic eruptions, but were only able to identify similar signals for the 4 April 1982, El Chichón (Mexico) eruption. In this case, a lower frequency spectral peak was observed at 3.70 mHz (270 s), along with the dominant peak was observed at 5.14 mHz (195 s). The uniqueness of a source process that excites just two distinct global Rayleigh waves with normal mode frequencies and the consistency of the lower frequency peak near 3.70 mHz led to the hypothesis that the signal resulted from coupling of eruption-excited atmospheric oscillations with the solid Earth (Kanamori & Mori 1992; Widmer & Zürn 1992). To the best of our knowledge, prior to our study, observations of these spectral peaks in microbarograph records have only been reported following the 1982 El Chichón eruption at Piñon Flat (California) and College Magnetic Observatory (Alaska), both over 1000 km from the volcano (Widmer & Zürn 1992).

Given the paucity of high signal-to-noise observations, current understanding of atmospheric modal excitation and its coupling with the solid Earth is principally informed by theory. Several studies have noted that characteristic temperature profiles in the atmosphere predict a fundamental acoustic-gravity mode near 3.68 mHz (Jones & Georges 1976; Tahira 1995; Dahlen & Tromp 1998; Lognonné *et al.* 1998; Watada & Kanamori 2010), which corresponds to the lower frequency peak excited by the Pinatubo and El Chichón eruptions. Tahira (1995) modelled this oscillation as an acoustic-gravity standing wave at frequencies of 3.64–3.69 mHz with an evanescent upper boundary and a wavelength λ of approximately four times the height of the mesopause ($\lambda = 380$–400 km). Similarly, the first atmospheric overtone of this mode occurs at 4.40 mHz, but modelling suggests it should attenuate much more rapidly than the fundamental mode due to energy leakage from the upper mesophere (Lognonné *et al.* 1998) as well as its lower intrinsic quality factor Q. Lognonné *et al.* (1998) estimates Q to be 114.7 for the 3.68 mHz mode and 21 for the 4.40 mHz mode (Dahlen & Tromp 1998; table 8.3). Therefore, it is unclear why this frequency was the dominant excitation for the 1991 Pinatubo eruption or why it was absent for the 1982 El Chichón eruption. Similarly, open questions remain regarding the distance at which these atmospheric modes can be directly observed in microbarograph records (Kanamori *et al.* 1994).

In this study, we leverage instrumentation improvements across the modern GSN to document global observations of the excitation of 3.72 mHz Rayleigh waves following the 2022 Hunga Tonga eruption. We first perform spectral analysis on the event and identify the amplitude and frequency of spectral peaks excited by the event across the world. We then use these observations of the Hunga Tonga eruption to determine Q for the spectral peak at 3.72 mHz. Next, we compare amplitudes of spectral peaks excited by the 1991 Pinatubo eruption to the 2022 Hunga Tonga eruption. Finally, we examine microbarograph records across the GSN following the 2022 Hunga Tonga eruption to search for the excitation of predicted atmospheric normal modes (e.g. Tahira 1995; Lognonné *et al.* 1998; Watada & Kanamori 2010).

GLOBAL OBSERVATIONS OF THE HUNGA TONGA ERUPTION

We examine all available long-period, high-gain, vertical-component (channel LHZ; 1 sample s^{-1}) seismic data recorded on the primary sensors (location code 00) across the GSN for the 1991 Pinatubo and 2022 Hunga Tonga eruptions. We have restricted our attention to vertical-component data as the signals of interest have a better signal-to-noise ratio (SNR) due to their lower sensitivity to tilt noise over the horizontal components (Beauduin *et al.* 1996). The GSN currently consists of 140 VBB high-dynamic-range seismic stations (Fig. 1) capable of recording ground motions with frequency contents spanning diurnal Earth tides (0.0115 mHz) to high-frequency seismic signals up to many tens of Hz. In the last two decades, many GSN stations have been augmented with additional geophysical instrumentation, including microbarographs (Fig. 1, blue). This makes it possible to examine the joint excitation of both the seismic and atmospheric modes for 2022 Hunga Tonga eruption. For this eruption, 112 of the 140 GSN stations recorded suitable vertical-component long-period seismic data for this analysis (e.g. no outages or significant data gaps).

The global excitation of the Earth from the Hunga Tonga eruption is readily observed in both microbarograph (Fig. 2a) and seismic data (Fig. 2b) with initial observations of these arrivals reported in Matoza *et al.* (2022) and Yuen *et al.* (2022). To illustrate different phases, Fig. 3 shows the vertical waveforms as recorded by GSN station ANMO (Albuquerque, New Mexico) for the microbarograph (Fig. 3a) as well as the vertical-component seismic (Fig. 3b), which are located approximately 9500 km from Honga Tonga. In Fig. 3, seismic data are filtered into bands of 10–40 mHz (green), 3–50 mHz (orange) and 3–5 mHz (red). *P* waves and surface waves with dominant energy above 10 mHz are the first arrivals at GSN stations following the event (Figs 2a and 3b; Matoza *et al.* 2022). Body-wave arrivals are immediately followed by oscillations below 5 mHz that visually appear monochromatic and that 'ring' for over 15 hr following the eruption (Fig. 3b, red). The atmospheric Lamb acoustic-gravity wave from the eruption is clearly seen in GSN

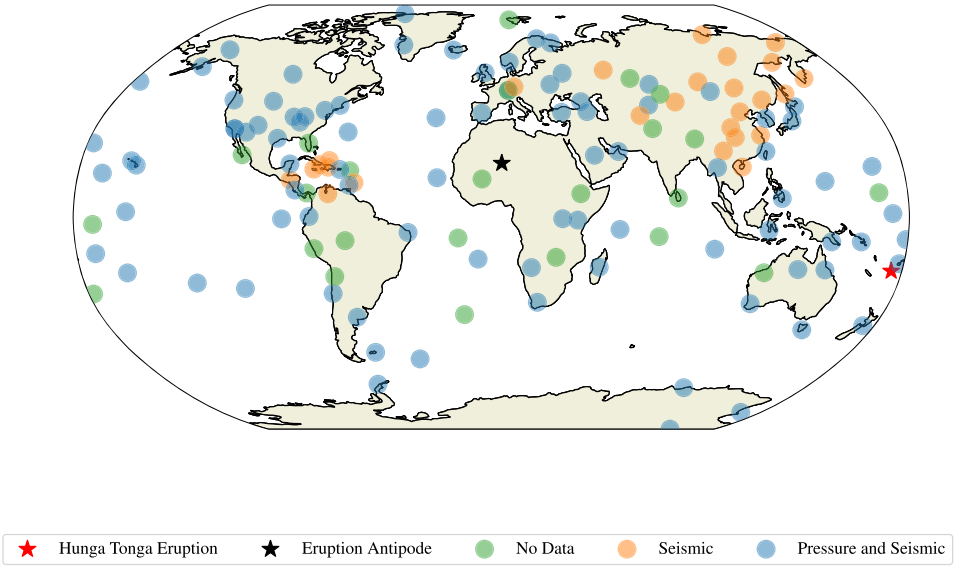

Figure 1. Map of the Global Seismographic Network (GSN) which includes the USGS Caribbean network (network code CU), the IRIS/IDA network (network code II), the IRIS/USGS network (network code IU), and the New China Digital Seismograph Network (network code IC; ASL 1992). Stations from these networks that did not provide data (e.g. station was down) during the event are depicted by green circles. Stations with both a microbarograph and seismometer are depicted by blue circles. Stations with only a seismometer are depicted by orange circles. We have included the location of the Hunga Tonga eruption (red star) as well as the antipode (black star).

microbarograph data (Fig. 2a) and travels at a global average velocity of 310 m s^{-1} (Matoza *et al.* 2022; blue line in Fig. 2a), closely followed by infrasonic arrivals ($f > 0.01$ Hz). Many infrasound signals generated by explosions (e.g. Edwards *et al.* 2007; Matoza *et al.* 2019; Anthony *et al.* 2022) produce ground motions (Fig. 3b, green) that are induced by these atmospheric perturbations (Fig. 3a) through local pressure deformation of the solid Earth. However, for atmospheric signals with lower frequency content (<3 mHz) it is possible that Newtonian attraction can be the dominate signal (Zürn & Wielandt 2007). The comparatively low velocity of the acoustic signals, one order of magnitude below the longer-period Rayleigh wave phase velocities of the Earth, implies that these pressure changes do not couple efficiently into an elastic surface wave (e.g. Kanamori & Mori 1992; Watada & Kanamori 2010).

SOLID EARTH NORMAL MODES

To characterize the extended lower frequency harmonic oscillation (i.e. normal modes), we process vertical-component seismic data to form spectral estimates between 3 and 6 mHz. We use 15-hr data segments (1.1Q cycles for $Q = 190$; Dahlen 1982) starting at 04:14:00 15 January 2022 UTC for the Hunga Tonga eruption and 06:30:00 15 June 1991 UTC for the Pinatubo eruption. For each data segment, we remove a least-squares linear trend, apply a Kaiser window taper with a β shape factor of 2π (Harris *et al.* 2020), and zero-pad the data to the next power of 2 (in this case 2^{16} samples). We then compute the discrete Fourier transform (DFT) and remove the instrument response in the appropriate band via spectral division. This yields a sample spacing of is 0.015 mHz in the frequency domain. An example of these spectra across the GSN for the Hunga Tonga eruption is shown in Fig. 4. For reference we include the frequencies of spheroidal modes in the 3.6 mHz region calculated from Mineos (Masters *et al.* 2014) using the Preliminary Reference Earth Model (PREM; Dziewonski & Anderson 1981). While different models of the Earth could produce different frequencies and quality factors (Montagner & Kennett 1996), we only use eigenfrequencies computed by PREM as these are used in Lognonné *et al.* (1998). Beyond the model being used, not accounting for Coriolis coupling (Masters *et al.* 1983) or crustal corrections (Lekić *et al.* 2010) could produce differences between the estimated frequency and those observed, however we are only using the reference frequencies for mode identification and therefore did not apply these additional corrections. We have also included the frequencies of the atmospheric modes between the solid Earth modes ${}_0S_{28}$–${}_0S_{29}$ (3.68 mHz, orange) and ${}_0S_{36}$–${}_0S_{37}$ (4.40 mHz, green) from Lognonné *et al.* (1998). In describing the atmospheric modes, we use the notation of Dahlen & Tromp (1998; section 8.8.12), where ${}_0S_l$–${}_0S_{l'}$ indicates the atmospheric mode with a frequency lying between the solid Earth fundamental modes ${}_0S_l$ and ${}_0S_{l'}$, and l and l' are angular degree values.

Fig. 4 shows obvious spectral peaks in the 3.5–3.8 mHz frequency band at nearly every GSN station; peaks near 4.4 mHz, however, are less clear. To quantify this excitation, we estimate the SNR of the excitation in the 3.5–3.8 mHz and 4.3–4.6 mHz bands using the peak amplitude within these bands as the signal and the peak amplitude in the 4.0–4.3 mHz and 5.0–5.3 mHz bands as the noise, respectively. Of the 112 stations considered, we find that 97 (blue, Fig. 4) recorded oscillations near 3.7 mHz with a SNR greater than 3. In contrast, only seven stations had a spectral peak with SNR greater than 3 near 4.4 mHz. Due to lack of high SNR observations, we do not consider the 4.4 mHz peak in subsequent peak frequency, amplitude or attenuation analysis.

We plot the amplitude (Fig. 5a) and corresponding peak frequency (Fig. 5b) between 3.5 and 3.8 mHz across the GSN. Stations with SNR < 3 in this band are plotted as squares to indicate that we have less confidence in the measurements. Excluding these stations, we estimate this mode has a mean frequency of 3.72 mHz with a standard deviation of 0.0164 mHz (roughly the sample spacing in our spectra; 0.0152 mHz) by way of estimating the frequency of the peak. Notably, this frequency aligns closely with the solid Earth

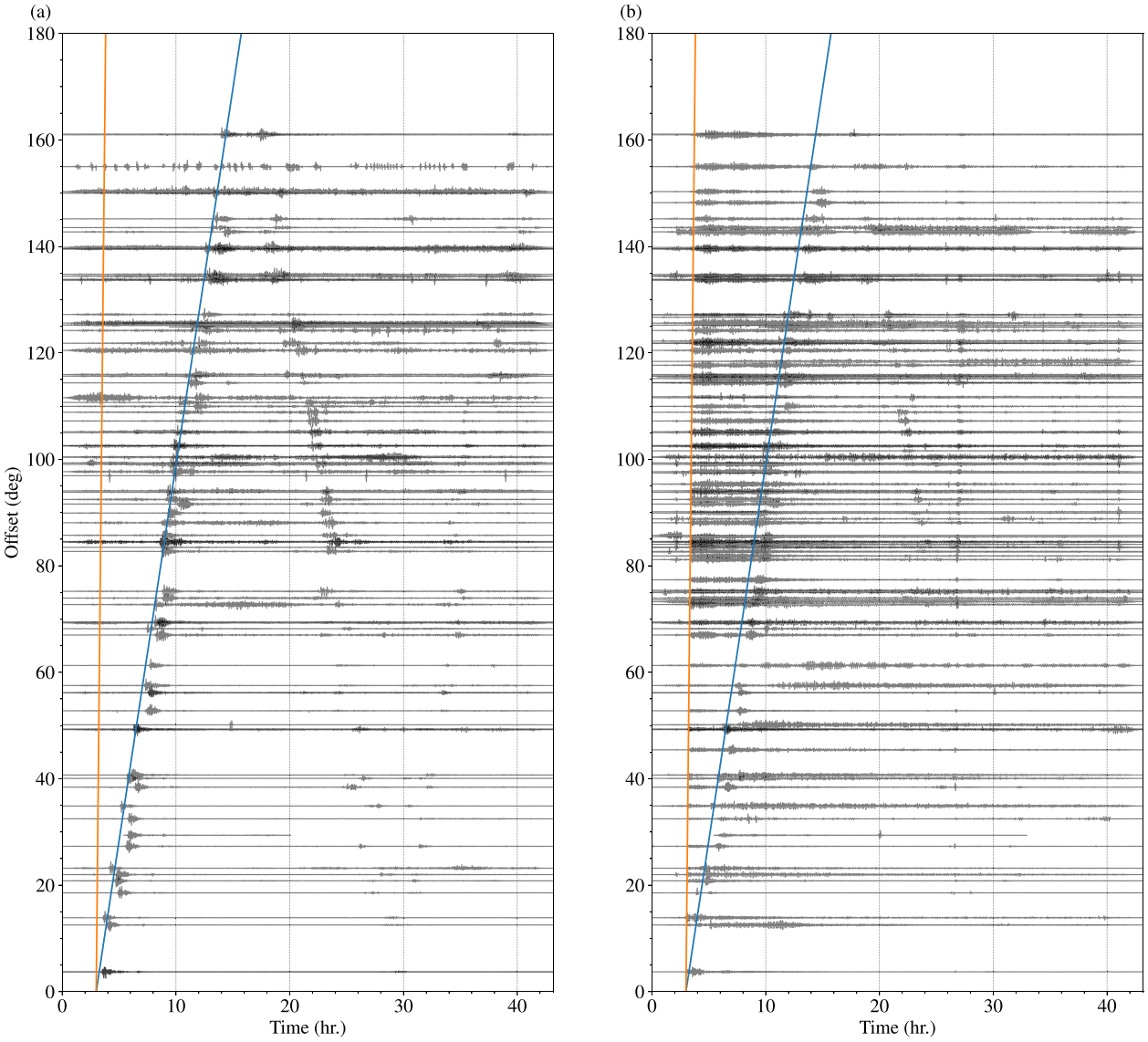

Figure 2. (a) Bandpass filtered record section from 100 to 1 mHz of microbarographs (channel LDO) in the Global Seismographic Network (GSN) with a starting time of 00:00:00 15 January 2022, UTC. (b) Same as (a), but for the long-period vertical-component seismic data (channel LHZ). For reference we have included the predicted arrival time of a Lamb wave travelling at 310 m s^{-1} (blue) as well as a Rayleigh wave travelling at 4000 m s^{-1} (orange).

mode ${}_0S_{29}$ (3.72 mHz) as calculated from PREM (Dziewonski & Anderson 1981). Stations PFO (Piñon Flat, CA) and ADK (Aleutian Islands, AK) are notable outliers with peak frequencies of 3.63 and 3.65 mHz, respectively (Fig. 5b) which more closely align with the frequency of ${}_0S_{28}$ (3.63 mHz).

Amplitude measurements across the GSN are more variable than peak frequency observations (Fig. 5a). The median spectral amplitude was 0.49 nm s^{-2} with a standard deviation of 0.45 nm s^{-2}. Amplitudes at most (84 per cent) stations are less than 0.6 nm s^{-2}, but we observe larger ($>$1.0 nm s^{-2}) ground motions across many of the southwest Pacific islands, central Africa, and at the station PAB (San Pablo, Spain). We did not attempt to correct for any excitation pattern by way of stacking as the mode was excited at all stations (e.g. Dahlen & Tromp 1998; section 10.6). Following Masters *et al.* (1982) we include these values as a function of the antipode of the great circle through the station and the Honga Tonga eruption in Fig. S1.

Estimate of attenuation: We estimate Q of ${}_0S_{29}$ (3.72 mHz) following the eruption by measuring the decay of spectral estimates at stations across the GSN in the 3.65–3.78 mHz band in subsequent time windows following the methodology of Sailor & Dziewonski (1978). We use this method as it does not require information about the source–time function (which at the time of this writing was unavailable), which would be required to produce synthetics used to estimate attenuation (e.g. Talavera-Soza & Deuss 2020). We consider a 30-hr record of data following the eruption and calculate spectra in 15-hr windows that move through the record in 1-hr steps (Fig. S2). In total, we calculate 16 spectra for each GSN station. We then estimate the average power (P_{avg}) from each spectrum in our record using a trapezoid rule integration approach (Sailor & Dziewonski 1978). After estimating the average power we estimate the slope m of $\ln(P_{\mathrm{avg}})$ from each time window as a function of time. This slope provides an estimate of $Q = -2\mathrm{p}/mf_{\mathrm{avg}}$, where f_{avg} is taken to be the average frequency in the band. To quantify how

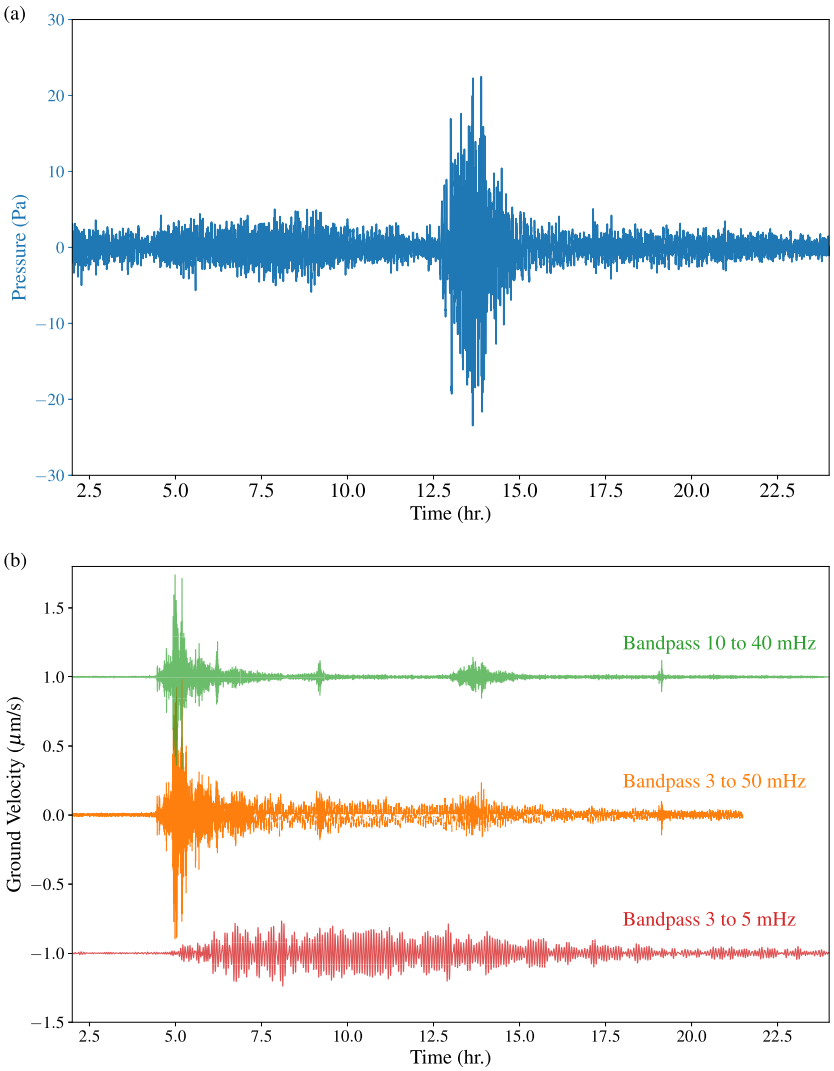

Figure 3. (a) Time-series of pressure as recorded by the microbarograph at GSN station ANMO (Albuquerque, New Mexico; 9524 km from Hunga Tonga) after bandpass filtering from 3 to 50 mHz. The times are relative 00:00:00 15 January 2022, UTC. (b) Time-series of the vertical seismic records as recorded by the primary sensor (location code 00) at GSN station ANMO after bandpass filtering from 10 to 40 mHz (green), 3 to 50 mHz (orange) and 3 to 5 mHz (red). All three traces are offset vertically on the plot for clarity.

well the decay of the mode is modelled by the linear regression, we also estimate the goodness of fit by estimating the residual between the data and linear regression in the least squares sense as decay of the natural logarithm of the average power should be approximately linear.

Estimates of Q for individual stations for the Honga Tonga eruption's excitation of ${}_0S_{29}$ are plotted in Fig. S3. We consider stations with a residual less than 1 to be consistent with the exponential decay of ${}_0S_{29}$ and plot these stations as circles. In Fig. S4 we include the Q estimates as a function of the antipodes of a great circle between the station and the Hunga Tonga eruption (Masters *et al.* 1982). If we consider only stations with a residual below 1, we estimate a mean Q of 332 with a standard deviation of 101, which is significantly greater than the 186.9 (with a standard deviation of 5) predicted by PREM (Dziewonski & Anderson 1981). Our attenuation measurement has relatively high scatter across the GSN stations and we do not observe clear spatial (Fig. S3) or great circle (Fig. S4) trends indicative of sensitivity to mantle structure. The method of Sailor & Dziewonski (1978) is weakly dependent on window size; however, we consistently obtain higher Q values than predicted by PREM even when adjusting the window between 10 and 20 hr.

Comparison to 1991 Pinatubo Eruption: Although the GSN was still in its infancy in 1991, 17 stations that recorded the 2022 Honga Tonga event also recorded the Pinatubo eruption (Fig. 6). To eliminate any stations that did not record solid Earth modes excited by either eruption with low SNR, we removed all spectra with a peak amplitude greater than 0.6 nm s^{-2} in the 3.9–4.1 mHz band and greater than 0.35 nm s^{-2} in the 3.0–3.4 mHz band, as these spectra were dominated by noise. To show differences in the frequencies that were excited between the Pinatubo and Hunga Tonga eruptions, we scale the Hunga Tonga spectra (Fig. 6, blue) at each station so that the amplitude of the peak spectra between 3 and 6 mHz is identical to the Pinatubo spectra (Fig. 6, brown). The scale factors applied to the Hunga Tonga spectra are shown in the right-hand side of the figure.

We find that when stacking all available GSN stations (Fig. 7), both the 1991 Pinatubo eruption (orange; 16 stations in stack) and

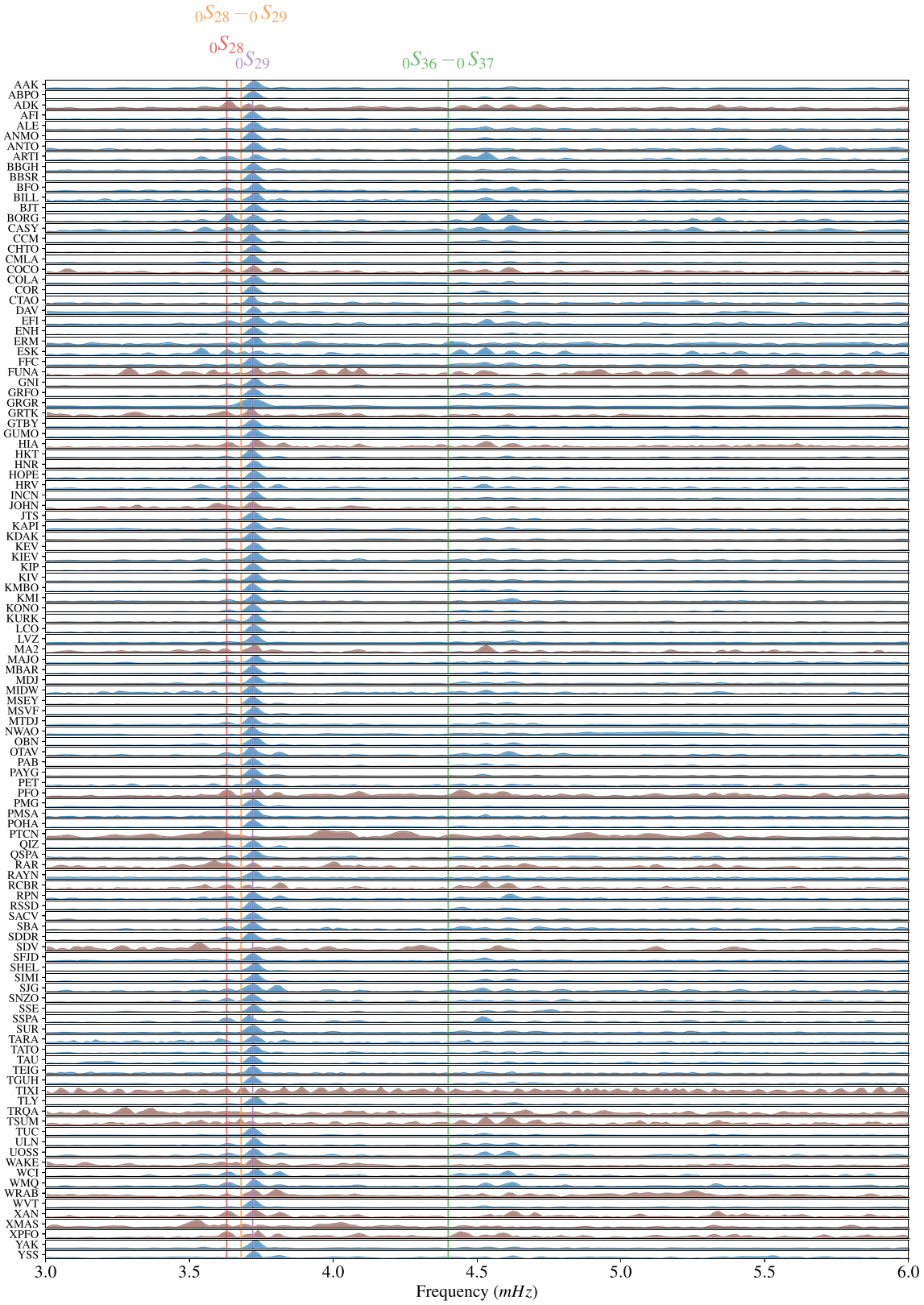

Figure 4. Vertical-component spectra from 15 hr of data starting at 04:14:00 15 January 2022, UTC for all primary (location code 00) seismometers (channel code LHZ) across the Global Seismographic Network. Stations that recorded the 3.7 mHz signal with a signal-to-noise ratio (SNR) greater than 3 are shown in blue, while stations with a lower SNR are shown in brown. For reference we include the frequencies of $_0S_{28}$ (3.63 mHz, red) and $_0S_{29}$ (3.72 mHz, purple) as estimated by the Preliminary Reference Earth Model (PREM; Dziewonski & Anderson 1981) as well as the atmospheric modes $_0S_{28}$–$_0S_{29}$ (3.68 mHz, orange) and $_0S_{36}$–$_0S_{37}$ (4.40 mHz, green) from Lognonné *et al.* (1998).

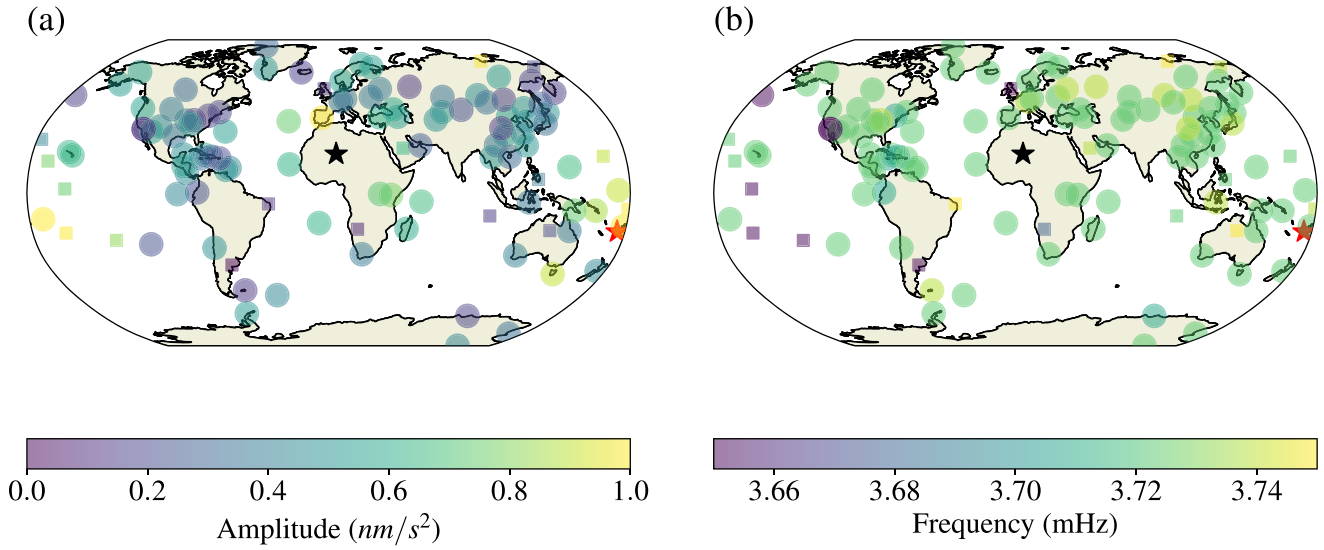

Figure 5. (a) Maximum amplitude of spectra in the 3.5–3.8 mHz band for 12 hr data starting at 04:14:00 15 January 2022, UTC for all primary (location code 00) seismometers (channel code LHZ) across the Global Seismographic Network. Stations with signal-to-noise ratio (SNR) greater than 3 are denoted by circles, and stations with an SNR less than 3 are denoted by squares. The location of the Hunga Tonga eruption is denoted by a red star, and the antipode is depicted by a black star. (b) Same as (a), but for the frequency where the peak amplitude occurred.

the 2022 Hunga Tonga eruption (green; 112 stations in stack) predominantly excited the solid Earth fundamental mode ${}_0S_{29}$ (3.72 mHz). However, we find that the excitation of ${}_0S_{29}$ was more than 11 times larger for the Hunga Tonga eruption when all stations that recorded the event are included. When considering the 17 individual stations that recorded both events (Fig. 6), 10 recorded peak amplitudes that were more than five times larger for the Hunga Tonga event.

The 2022 Hunga Tonga eruption excited additional fundamental modes of the Earth (as calculated from PREM; Dziewonski & Anderson 1981) that are not visible in the Pinatubo eruption GSN stack (Fig. 7) including ${}_0S_{28}$ (3.63mHz), ${}_0S_{30}$ (3.81 mHz), ${}_0S_{38}$ (4.53 mHz) and ${}_0S_{39}$ (4.62 mHz). We note that although we do not observe any peaks near 4.44 mHz (e.g. Widmer & Zürn 1992) for the Pinatubo eruption when stacking the 16 stations, peaks around this frequency are clearly observed at individual stations (Fig. 6).

ATMOSPHERIC MODES

We processed the atmospheric pressure data (location code LDO or LDI) at all 89 GSN stations that had microbarographs using the same procedure as the seismic data, described above (Fig. 4) except we use a 26-hr time-series to account for the slower velocity of the atmospheric waves. Although this is longer than the 1.1 Q-cycle time window (Dahlen 1982), this is necessary because it takes the Lamb acoustic-gravity wave nearly 18 hr after the eruption to reach the antipode (e.g. Fig. 2a). All pressure data used were recorded by well calibrated pressure transducers (location codes 31 or 00). Although all operating microbarographs recorded the initial Lamb wave and infrasound signals produced by the eruption, the only stations where the SNR of the microbarograph was above 3 in the 3.5–3.8 mHz band were MSVF (Monasavu, Fiji) and OBN (Obninsk, Russia). Data from station OBN were dominated by noise and produced a false positive, as visual inspection doesn't show a distinct peak in the 3.5–3.8 mHz region. Station AFI (Afiamalu, Samoa) potentially recorded the excitation of a peak in the 3.5–3.8 mHz band, but it had relatively poor SNR (Fig. S5) and the lack of excitation could have also come from source directivity (Kim *et al.* 2012). We did observe an even lower frequency signal (approximately 2.78 mHz) at station AFI that was also observed on an AGBOM microbarograph in Samoa (Fig. S5). We do note that no microbarographs recorded a spectral peak with an SNR greater than 3 in the 4.3–4.6 mHz region (Fig. S6).

Pressure oscillations around 3.7 mHz at MSVF do not appear until about 40 min following the eruption and occur in several episodic pulses roughly coincident with seismic energy (Figs 8 and 9). The first pulses following the eruption show pressure oscillations that are in phase with of seismic accelerations, but this does not hold true for later arrivals. Applying a least-squares pressure correction, similar to the method described in Zürn & Widmer (1995) and further discussed in Zürn & Meurers (2009), we found only a 33 per cent reduction in variance (Fig. 8, green). Our estimated correction coefficient was 13.3 $nm\,s^{-2}\,hPa^{-1}$. This value is much larger than any of those estimated by Zürn & Meurers (2009) in their table 1 and opposite in sign. Their values are all near 4 $nm\,s^{-2}\,hPa^{-1}$. The pressure and seismic records at MSVF provide a local example near the notch frequency discussed in Zürn & Wielandt (2007). We note here again that seismic energy bandpass filtered around ${}_0S_{29}$ decays more slowly than would be predicted by PREM (Fig. 9c).

DISCUSSION

We suggest that these pressure oscillations at 3.71 and 3.73 mHz recorded on MSVF represent the first direct observation of excitation of the fundamental mode of the atmosphere since microbarograph observations at Piñon Flat (California) following the 1982 El Chichón eruption (Widmer & Zürn 1992). Coupling of this atmospheric mode into the solid Earth was modelled by several studies to explain the seismic observation following the 1991 Pinatubo eruption (Tahira 1995; Lognonné *et al.* 1998; Watada &

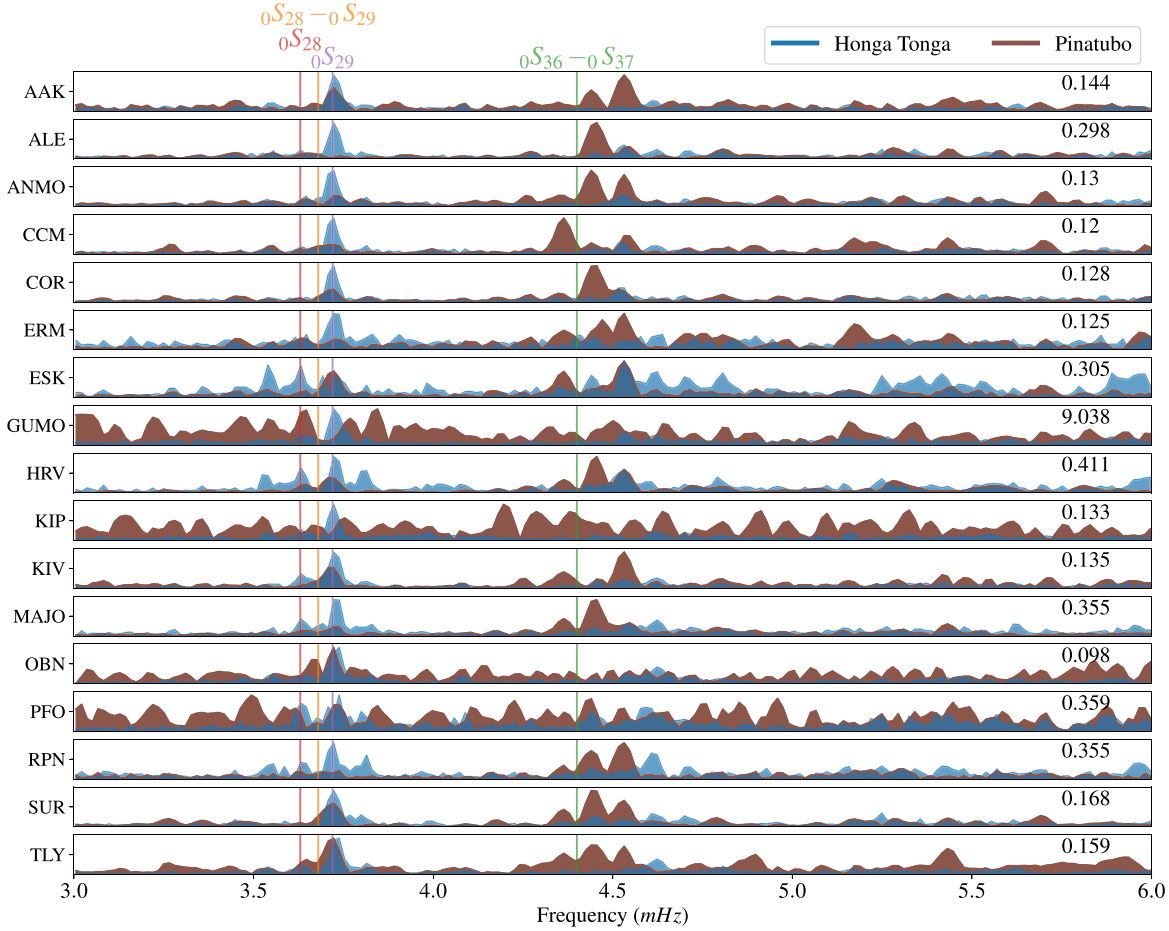

Figure 6. Vertical-component acceleration spectra from 12 hr of data starting at 04:14:00 15 January 2022 UTC for all primary (location code 00) seismometers (channel code LHZ) at 17 stations of the Global Seismographic Network (blue) and for the Pinatubo eruption starting at 06:30:00 15 June 1991 (brown). Spectra were normalized to the peak amplitude in the 3–6 mHz frequency band. For reference we include the frequencies of $_0S_{28}$ (3.63 mHz, red) and $_0S_{29}$ (3.72 mHz, purple) as estimated by the Preliminary Reference Earth Model (PREM; Dziewonski & Anderson 1981) as well as the atmospheric modes $_0S_{28}$–$_0S_{29}$ (3.68 mHz, orange) and $_0S_{36}$–$_0S_{37}$ (4.40 mHz, green) from Lognonné *et al.* (1998). The numbers on the right-hand side indicate the ratio of the peak amplitude of the Pinatubo event relative to the peak amplitude of the Hunga Tonga eruption in the 3–6 mHz frequency band.

Kanamori 2010). However, nearby direct pressure observations during the eruption lacked sufficient timing accuracy to enable a direct observation of this mode (Widmer & Zürn 1992). Other studies have observed nearfield atmospheric oscillations at different frequencies (e.g. Kanamori *et al.* 1994), but the interpretations and robustness have been questioned (Watada & Kanamori 2010). For the Hunga Tonga eruption, our observation of the microbarograph oscillation at ∼3.7 mHz is in phase with the vertical seismic acceleration at MSVF (Fig. 8). As we discuss below, we observe a similar atmospheric excitation from a second, regional (∼68 km) microbarograph located in Tonga and demonstrate that the observed attenuation of 3.7 mHz pressure variations at this station is consistent with theoretical modelling of the fundamental mode of Earth's atmosphere. Therefore, our observations following the 2022 Hunga Tonga eruption support these previous models that global excitation of $_0S_{29}$ following large volcanic eruptions results from local excitation of the fundamental mode of the atmosphere and subsequent coupling into the solid Earth.

We estimate the Q of $_0S_{29}$ across the GSN following the 2022 Hunga Tonga eruption and find $Q = 332 \pm 101$ which is much larger than the $Q = 186.9$ for mode $_0S_{29}$ predicted by PREM. We interpret the higher measured values of Q as resulting from an extended eruption duration coupled with the relatively slow decay of the induced atmospheric pressure oscillations. For instance, Poli & Shapiro (2022) estimate the eruption duration to be more than 6000 s, which is about 40 times longer than the rupture duration of the M_w 9.0 2011 Tohoku earthquake (Ammon *et al.* 2011). Lognonné *et al.* (1998) estimate Q of the fundamental atmospheric mode to be 114.7. Therefore, even an impulsive excitation of this atmospheric mode will generate pressure oscillations at Earth's surface for several hours and Rayleigh waves (excited from these pressure oscillations) will continue to be generated near the volcanic source even after the eruption has ceased. We also estimated elevated Q values for the Pinatubo event ($Q = 399 \pm 93$), which we note agrees with the Hunga Tonga estimate and is also substantially higher than predicted by PREM (Fig. S7). However, since only a few stations were available, our confidence in these estimates is less than for the Hunga Tonga event.

We directly record this extended atmospheric source duration in the raw pressure data at MSVF, where oscillations around 3.7 mHz are recorded for several hours following the eruption (Fig. 9b). Although not a GSN station, we did observe similar 3.7 mHz pressure

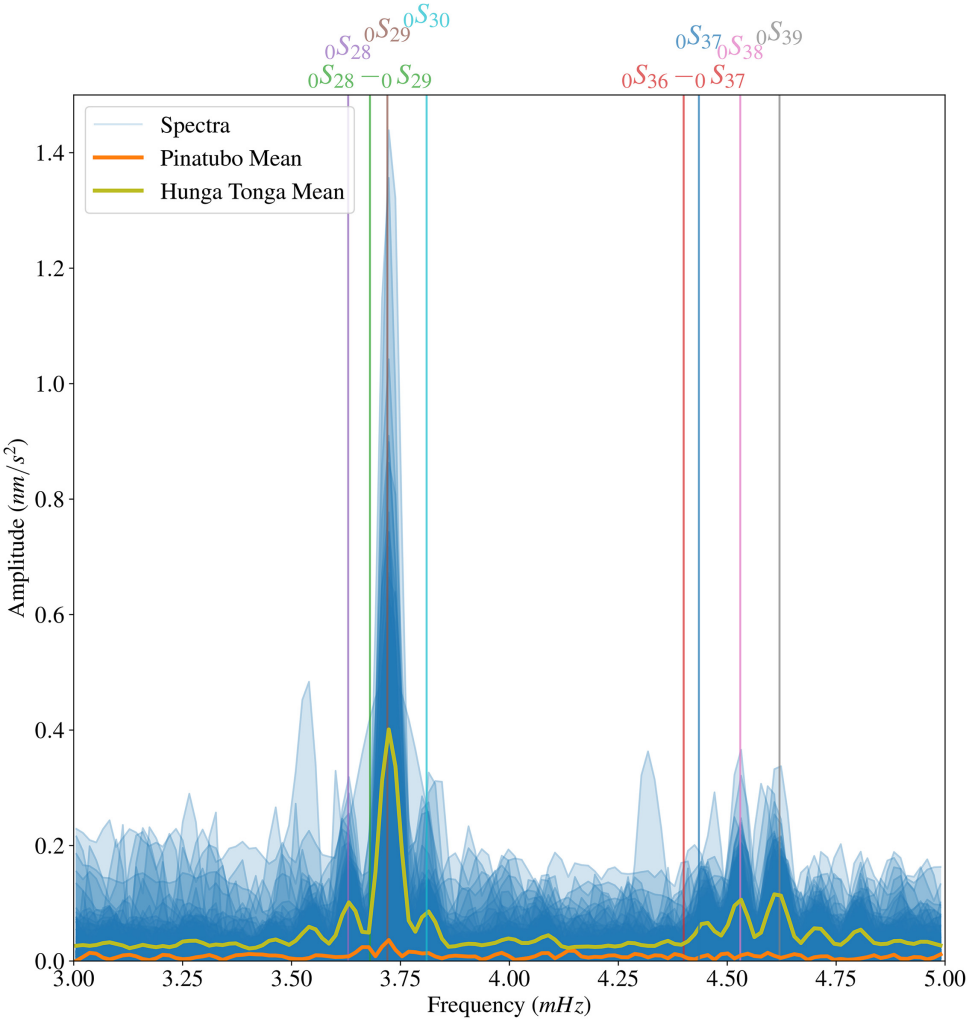

Figure 7. Vertical-component spectra from 12 hr of data for the Hunga Tonga eruption starting at 04:14:00 15 January 2022, UTC for all primary (location code 00) seismometers (channel code LHZ) across the Global Seismographic Network (blue) as well as the mean spectra of all stations for the Hunga Tonga event (green) and the Pinatubo event (orange). We have removed all spectra that had amplitudes greater than 0.6 nm s^{-2} in the 3.9–4.1 mHz band and 0.35 nm s^{-2} in the 3.0–3.4 mHz band because these are spectra that are dominated by noise. For reference we include the frequencies of $_0S_{28}$ (3.63 mHz, purple), $_0S_{29}$ (3.72 mHz, brown), $_0S_{30}$ (3.81 mHz, cyan), $_0S_{37}$ (4.43 mHz, dark blue), $_0S_{38}$ (4.53 mHz, pink) and $_0S_{39}$ (4.62 mHz, grey) as estimated by the Preliminary Reference Earth Model (PREM; Dziewonski & Anderson 1981) as well as the atmospheric modes $_0S_{28}$–$_0S_{29}$ (3.68 mHz, green) and $_0S_{36}$–$_0S_{37}$ (4.40 mHz, red) from Lognonné *et al.* (1998).

oscillations on a barometer located in Tonga from the Australian Government Bureau of Meteorology (AGBOM, Fig. 10) roughly 68 km from the eruption. Here, the peak frequency of excitation is 3.73 mHz (with a subpeak at 3.70 mHz) and peak pressure exceeding 100 Pa and can be visually observed in raw pressure data for at least 9 hr following the eruption. We estimate Q of the fundamental mode of the atmosphere using pressure records in Tonga similarly to how we estimated Q of $_0S_{29}$ from seismic records. Because the signal decays faster, we instead consider only 12 hr and step through the data in half hour increments with 6-hr spectral windows. Using this technique, we arrive at a Q estimate of the atmosphere of 111.8, which is quite close to the modelled quality factor of $Q = 114.7$ (Lognonné *et al*. 1998; Fig. 11a).

Although the fundamental mode of the atmosphere is observed in pressure data at MSVF (755 km from the volcano), this mode is not observed at publicly available pressure sensors across the globe including at the GSN station RAR (Raratonga; approximately 1500 km from the volcano). While we potentially also observed this signal at AFI (Afiamalu, Samoa; approximately 831 km from the volcano), the SNR of the mode at that station was too low for us to definitively declare a detection there (Fig. S5). It is possible that the spatial area of atmospheric to ground coupling may be limited to a radius of less than 1000 km from the volcano. Notably, this is significantly larger than the 37 km radius modelled for the first atmospheric overtone (∼4.4 mHz) following the 1991 Pinatubo eruption (Kanamori & Mori 1992).

However, the long source–time function of the eruption could complicate our ability to understand the region of atmospheric to ground coupling. It is also possible that we are not able to resolve some pressure oscillations at more distant and azimuthally distributed sensors due to attenuation and higher background noise levels from wind or pressure source directivity (e.g. Kim *et al.* 2012). To our knowledge, the only previous observation of the fundamental atmospheric mode following an eruption was from the

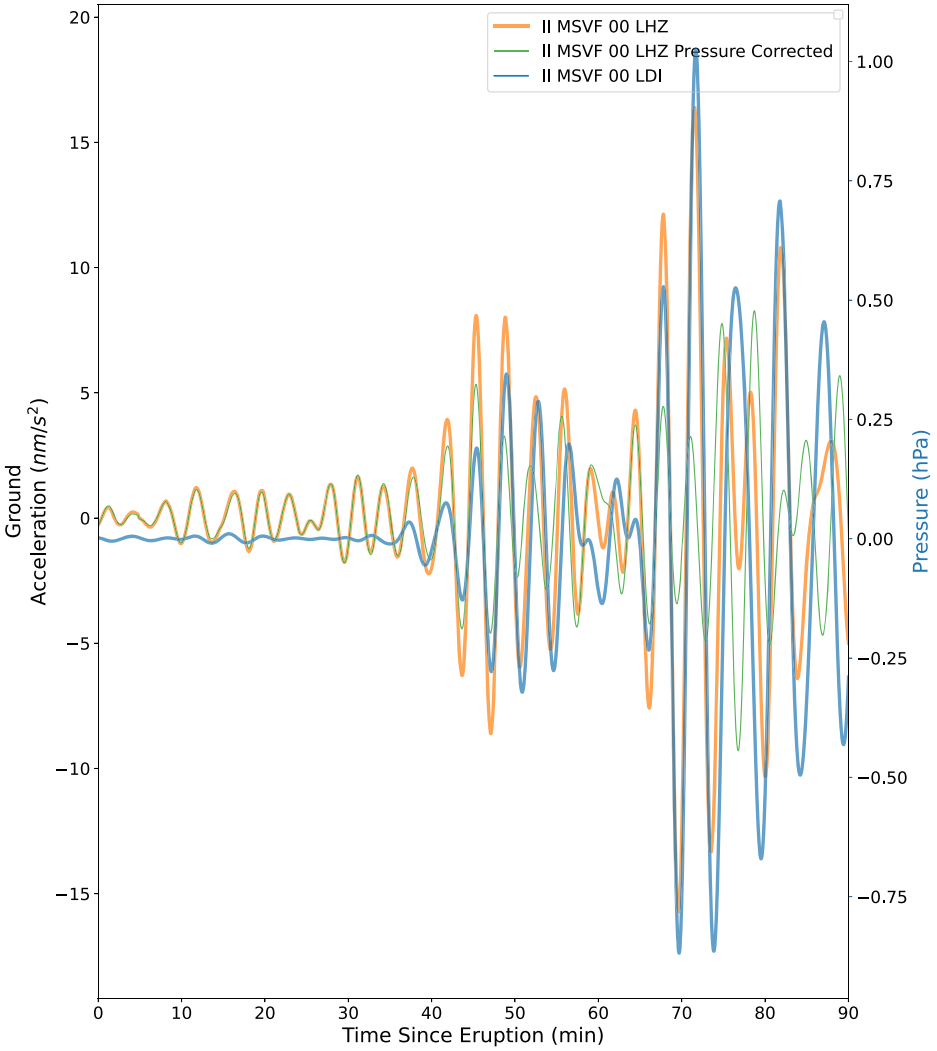

Figure 8. 90 min of time-series data from IRIS/IDA station MSVF (Monasavu, Fiji) starting at 04:14:00 15 January 2022, UTC for the microbarograph (channel: LDI, blue) and the vertical-component seismic data (channel: LHZ, orange) after filtering from 3 to 5 mHz. We also show the vertical seismic data after subtracting off a pressure correction coefficient of 13.3 $nm\,s^{-2}\,hPa^{-1}$ that was estimated by minimizing the sum of the squares (green). This pressure corrected data has a variance reduction of 33 per cent over the original acceleration data (orange).

1982 El Chichón eruption at PFO (Piñon Flat, California) at approximately 3000 km from the volcano (Widmer & Zurn 1992). Therefore, questions remain regarding the spatial extent to which the atmospheric excitation occurred.

We note that although we measure the peak frequency of the fundamental mode of the atmosphere at MSVF and in Tonga following the eruption of Hunga Tonga to between 3.71 and 3.73 mHz, the eigenfrequency of the mode is dependent on atmospheric structure and has been modelled to occur anywhere between 3.64 and 3.75 mHz depending on season and latitude (Tahira 1995; Watada & Kanamori 2010). A double-peak at 3.71 and 3.73 mHz is clearly observed in the spectra at MSVF, but this pattern is less clear on the Tonga microbarograph (Fig. 11). It is unclear what is causing the double-frequency peak of the fundamental atmospheric mode at MSVF. The robustness of this observation is also questionable given the relatively limited 12-hr data window, but is a curious feature in this dataset.

Although the fundamental mode of the atmosphere can vary slightly (∼0.1 mHz; Tahira 1995) based on atmospheric structure, we observe consistent excitation of the spheroidal solid Earth fundamental mode ${}_0S_{29}$ (3.72 mHz) for both the 2022 Hunga Tonga eruption and the 1991 Pinatubo eruption (Fig. 6). We note that the eigenfrequency we calculate for Pinatubo is slightly different than the 3.68 mHz (standard deviation of 0.02 mHz) reported by Widmer & Zürn (1992). This could be because Widmer and Zürn calculate spectra using 3-hr windows of data (Table 1 of Widmer & Zürn 1992), which is in contrast to our 12-hr windows of data. Although Widmer & Zürn (1992) made their measurements on gravimeters and this study mostly uses force-feedback seismometers (e.g. Streckeisen STS-1 s), it is unlikely that this could produce a difference in the measured eigenfrequency.

We observe that the amplitude of ${}_0S_{29}$ excited by the 2022 Hunga Tonga eruption was over an order of magnitude larger than the same excitation from the 1991 Pinatubo eruption. The reason for this observation is unclear but could be related to how effectively each eruption excited the atmosphere and enabled solid Earth coupling, the area over which atmospheric-to-solid Earth coupling occurred or potentially other differences in the source mechanisms

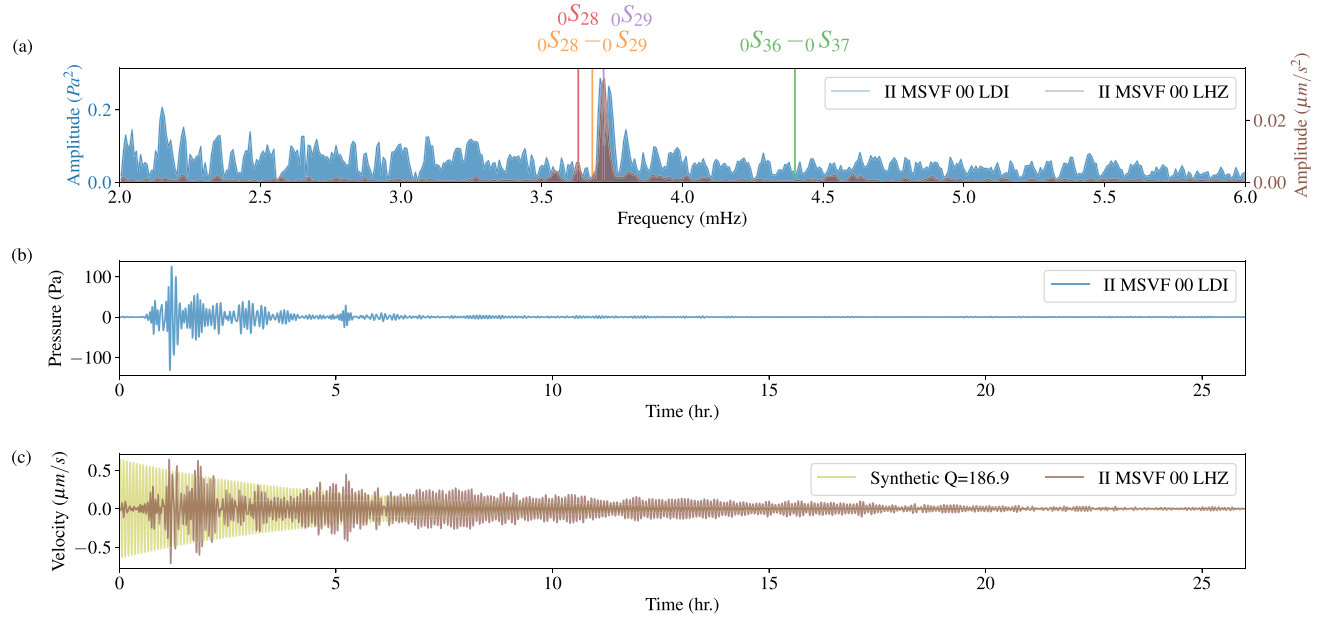

Figure 9. (a) Spectra for the microbarograph (blue) at IRIS/IDA station MSVF (Monasavu, Fiji) for 26 hr of data starting at 04:14:00 15 January 2022, UTC. Spectra for the vertical-component seismic data (brown) are also included. For reference we include the frequencies of $_0S_{28}$ (3.63 mHz, red) and $_0S_{29}$ (3.72 mHz, purple) as estimated by the Preliminary Reference Earth Model (PREM; Dziewonski & Anderson 1981) as well as the atmospheric modes $_0S_{28}$–$_0S_{29}$ (3.68 mHz, orange) and $_0S_{36}$–$_0S_{37}$ (4.40 mHz, green) from Lognonné *et al.* (1998). (b) Time-series for the pressure data used in after bandpass filtering between 2.5 and 5 mHz (a). (c) Time-series for the seismic data (brown) used in part (a) as well a synthetic decaying sinusoid with a $Q = 186.9$ (yellow) after bandpass filtering between 2.5 and 5 mHz.

between the two eruptions. This comparison is further complicated by the Pinatubo event being a subaerial volcano on land while the Hunga Tonga eruption was partially submerged (Pallister *et al.* 1992). The excitation of these low-frequency modes from the submerged nature of the Hunga Tonga eruption could be further complicated by taking place in a seawater environment (Thiéry & Mercury 2009).

We hypothesize that more efficient coupling between the atmosphere and the solid Earth may occur when the atmospheric eigenfrequency is closer to a fundamental solid Earth mode and this could potentially have contributed to the higher amplitude excitations of $_0S_{29}$ following the Hunga Tonga eruption. Using a model of the atmosphere during the 1991 Pinatubo eruption, Watada & Kanamori (2010) estimate the eigenfrequency of the atmospheric fundamental mode as 3.68 mHz. Although there are no direct observations of the eigenfrequency of the atmosphere during the Pinatubo eruption, this suggests that 3.71–3.73 mHz atmospheric resonance of the 2022 Hunga Tonga eruption (Fig. 11) may have been closer to the eigenfrequency of $_0S_{29}$ (3.72 mHz).

We also hypothesized that the extreme height of the eruption plume (≈55−58 km; Carr *et al.* 2022; NASA 2022) generated by the Hunga Tonga eruption may have also played a role by more strongly exciting the fundamental mode of the atmosphere compared to the 1991 Pinatubo eruption (plume height ≈35 km; NASA 2022). Watada & Kanamori (2010) model that up to 50 km, excitation of both the fundamental mode (∼3.7 mHz) and first overtone (∼4.4 mHz) of Earth's atmosphere becomes more efficient as the source altitude increases. Pressure oscillations (of unknown frequency content) following the 1991 Pinatubo eruption were observed 21 km from the volcano to have an amplitude of roughly 300 Pa (Kanamori & Mori 1992). In contrast, pressure oscillations between 2.5 and 5 mHz following the Hunga Tonga eruption are roughly 200 Pa at AGBOM (Fig. 10a) and 100 Pa MSVF (Fig. 9b). Therefore, these observations suggest that atmospheric pressure oscillations generated by the Tonga eruption may not have been appreciably larger than those generated by Pinatubo.

Although previous studies note that the dominant excitation of the 1991 Pinatubo event is near 4.44 mHz (e.g. Kanamori & Mori 1992; Widmer & Zürn 1992), we observe that the eigenfrequency of this peak is highly variable across different GSN stations (Figs 6 and 7). In contrast, the Hunga Tonga eruption appears to have excited several fundamental modes of the Earth in the 3.7 mHz region as well as the 4.4 mHz region. The signals we observe are still largely 'bi-chromatic,' as described in Widmer & Zürn (1992), but we can see that several frequencies are excited in both regions including frequencies that correspond to $_0S_{28}$, $_0S_{29}$, $_0S_{30}$, $_0S_{37}$, $_0S_{38}$ and $_0S_{39}$ (Fig. 7). We note that this excitation of several solid Earth modes outside of the fundamental mode and first overtone of the atmosphere is not anticipated from recent modelling (Watada & Kanamori 2010). This could be a result of variations in the atmosphere near the eruption (e.g. pressure and temperature) as well as source processes as the eruption occurred under water. We do not see any obvious change in the frequencies being excited based on the distance to the event or the antipode (Figs 5b and S1). These excitations may result from variations in the atmosphere which would produce different frequencies (Lognonné *et al.* 1998). While the excitation of these modes is interesting, modeling their generation using more realistic earth models (e.g. Bishop *et al.* 2021) could help to better understand these excitations and how the model can directly influence the excitation frequency.

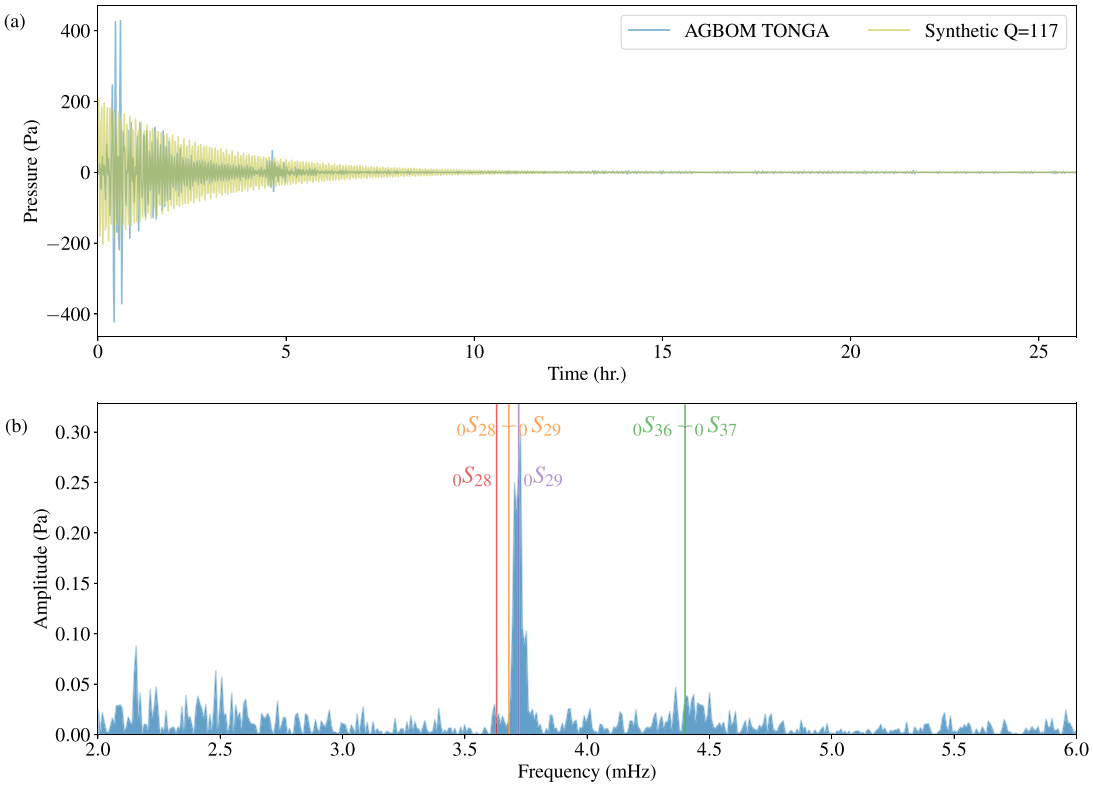

Figure 10. (a) 26 hr of time-series of pressure data from the Australian Government Bureau of Meteorology (AGBOM) barometer located in Tonga (about 68 km from eruption, latitude −21.1303, longitude −175.1967, blue) starting at 04:14:00 15 January 2022 UTC after bandpass filtering between 2.5 and 5 mHz. A synthetic decaying sinusoid with a $Q = 114.7$ and a peak amplitude of one-half the maximum of the blue time-series is shown in yellow. (b) Corresponding spectra from the time-series in (a). For reference we include the frequencies of $_0S_{28}$ (3.63 mHz, red) and $_0S_{29}$ (3.72 mHz, purple) as estimated by the Preliminary Reference Earth Model (PREM; Dziewonski & Anderson 1981) as well as the atmospheric modes $_0S_{28}$–$_0S_{29}$ (3.68 mHz, orange) and $_0S_{36}$–$_0S_{37}$ (4.40 mHz, green) from Lognonné *et al.* (1998).

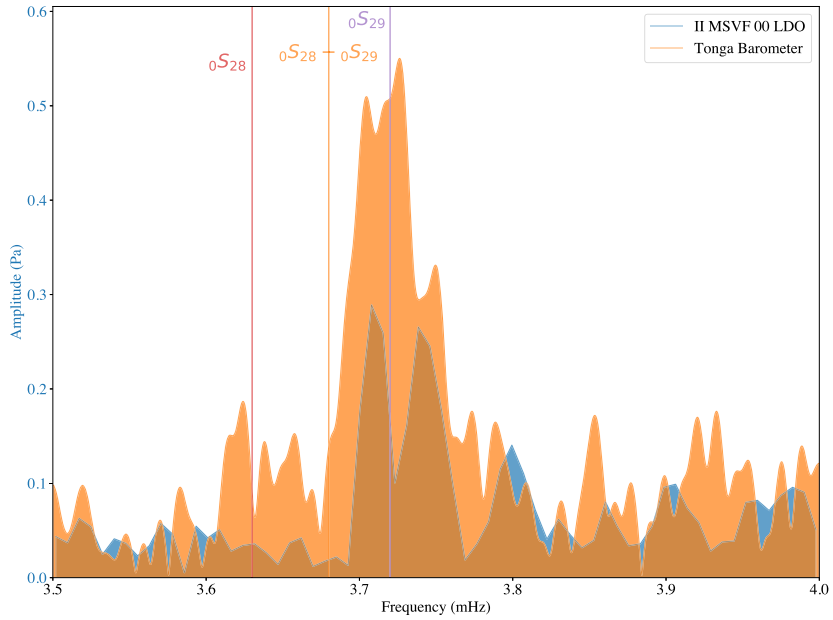

Figure 11. Spectra for the microbarograph (blue) at IRIS/IDA station MSVF (Monasavu, Fiji) for 26 hr of data starting at 04:14:00 15 January 2022, UTC. Spectra from a barometer located in Tonga (about 68 km from eruption, latitude −21.1303, longitude −175.1967, orange) are also included. For reference we include the frequencies of $_0S_{28}$ (3.63 mHz, red) and $_0S_{29}$ (3.72 mHz, purple) as estimated by the preliminary reference Earth model (PREM; Dziewonski & Anderson 1981) as well as the atmospheric mode $_0S_{28}$–$_0S_{29}$ (3.68 mHz, orange) from Lognonné *et al.* (1998).

CONCLUSIONS

The 15 January 2022 Hunga Tonga eruption provided the best opportunity since the 1991 Pinatubo eruption to record solid Earth normal modes generated through acoustic coupling of atmospheric normal modes. Similar to the 1991 Pinatubo eruption (and unlike earthquakes), when stacking ground motion spectra following the eruption we find unique 'bi-chromatic' excitation of solid Earth modes near the frequencies of 3.7 and 4.4 mHz. Because these frequencies correspond to the fundamental and first overtone frequencies of Earth's atmosphere, several models had been put forth following the Pinatubo eruption that the excitation of these discrete normal modes arose through acoustic coupling between the atmosphere and the solid Earth. Utilizing global seismic records as well as microbarograph records in proximity (<1000 km) to the eruption, we make several fundamental observations which largely support this modelling.

First, for the 2022 Hunga Tonga eruption, we measure the global quality factor, Q, of solid Earth normal mode ${}_0S_{29}$ to be 332 ± 101, which is significantly higher than predicted by the PREM model ($Q = 186.9 \pm 5$). This higher Q value is consistent with the extended seismic source duration presented in atmospheric-solid Earth coupling models. Secondly, we present pressure data recorded in proximity (<1000 km) to the eruption which display pronounced spectral peaks near 3.7 mHz. These measurements likely represent the highest fidelity recordings to date documenting excitation of the fundamental mode of Earth's atmosphere. At the closest micobarograph to the eruption (~68 km), pressure oscillations at 3.7 mHz exceed 200 Pa and we directly measure Q of these oscillations to be 111.8, which is close to what is predicted by theoretical modelling. At MSVF (Monasavu, Fiji), colocated seismic and pressure observations indicate that initial pressure and ground acceleration oscillations occur in phase. Taken together, these observations are consistent with the hypothesis that global observations of ${}_0S_{29}$ following the 1991 Pinatubo eruption resulted from excitation of a fundamental mode of the atmosphere, which subsequently coupled into the solid Earth. We show that only microbarographs in relatively close (<1000 km) proximity observe these pressure oscillations and suggest that this coupling may occur over a limited spatial scale. This explains why observations of Rayleigh waves following the eruption have traveltimes consistent with a source at the site of the eruption.

We also found many discrepancies between normal mode excitation following the two eruptions. Unlike the 1991 Pinatubo eruption, most individual seismic stations do not display spectral peaks in ground motion near 4.4 mHz and the overall dominant excitation (both in the atmosphere and solid Earth) occurred near 3.7 mHz. Although we found that the solid Earth mode ${}_0S_{29}$ (3.72 mHz) was excited by both eruptions, the excitation amplitude was roughly 11 times larger for the 2022 Hunga Tonga eruption than the 1991 Pinatubo eruption. The physical reason behind this observation is unclear, but it could be due to differences in source processes changing how the atmosphere was excited or differences in the regional atmospheric structure. We make several observations following the 2022 Hunga Tonga eruption that are not consistent with previous models (e.g. Lognonné *et al.* 1998), including the two spectral peaks in the pressure record at MSVF and the excitation of a suite of fundamental solid Earth modes following the eruption. This could be related to previous models using only 1-D radial Earth parametrizations, perhaps extending the methods of Bishop *et al.* (2021) to a global 3-D earth model would partially resolve this issue.

The 2022 Hunga Tonga eruption is likely only the third time we have been able to use seimometers to observe atmospheric modes coupling into Solid Earth normal modes. We are confident that these observations will help to better constrain modelling of some of the less understood processes associated with modal coupling between the atmosphere and solid Earth.

DATA AND RESOURCES

Most data used in this study were obtained through the facilities of the Incorporated Research Institutions for Seismology (IRIS)/U.S. Geological Survey (USGS) network (network code IU; ASL/USGS 1988), the New China Digital Seismograph Network (network code IC; ASL/USGS 1992), the Caribbean USGS Network (network code CU; ASL/USGS 2006), as well as the International Deployment of Accelerometers (IDA) network (network code II; Scripps Institution of Oceanography 1986). These data are freely available at the IRIS Data Management Center (DMC).

The Tonga barometer data used in Fig. 11 are available within the repository associated with this work (https://github.com/aringler-usgs/tonga_paper); that station is part of an Australian Aid project called Climate and Oceans Support Program in the Pacific (COSPPac) with stations across 13 Pacific Island countries. The maintenance, operations, and products of the tide and global navigation satellite systems (GNSS) stations within COSPPac are managed by Robert Greenwood (Australian Bureau of Meteorology) through the Pacific Sea Level and Geodetic Monitoring (PSLGM) project (http://www.bom.gov.au/pacific/projects/pslm/).

We relied heavily on the Python library ObsPy (Megies *et al.* 2011) as well as Cartopy (Met Office 2015).

The facilities of IRIS Data Services, and specifically the IRIS DMC, were used for access to waveforms, related metadata, derived products used in this study. IRIS Data Services are funded through the Seismological Facilities for the Advancement of Geoscience and EarthScope (SAGE) Proposal of the National Science Foundation (NSF) under Cooperative Agreement EAR-1261681.

The Global Seismographic Network (GSN) is a cooperative scientific facility operated jointly by the IRIS, the USGS and NSF, under Cooperative Agreement EAR-1261681.

RSM and HDO acknowledge NSF grant EAR-1847736.

SDA acknowledges support from Royal Society International Exchange grant IES\R2\202 007.

Any use of trade, firm or product names is for descriptive purposes only and does not imply endorsement by the U.S. Government.

ACKNOWLEDGMENTS

This work has benefited from discussions along with a helpful review of the manuscript by Charles Hutt. We thank an anonymous reviewer, Rex Baum, Ryan Gold, Barbara Ralston, Simon Schneider, Liam Tone and Rudolf Widmer-Schnidrig for careful reviews that improved the manuscript. We thank Toshiro Tanimoto for suggesting an amplitude comparison with synthetic seismograms which led us to investigate several other pieces. This work benefited greatly from discussions with coauthors involved in the preparation of Matoza *et al.* (2022).

AUTHOR CONTRIBUTIONS

A. T. Ringler: conceptualization, data curation, formal analysis, methodology, and writing; R.E. Anthony: conceptualization, data

curation, formal analysis, methodology, and writing; R.C. Aster: methodology and writing; T. Taira: conceptualization, methodology, and formal analysis; B.R. Shiro: writing; D.C. Wilson: writing; M. Haney: data curation, writing; S. De Angelis: formal analysis, writing; C. Ebeling: writing; R.S. Matoza: methodology and writing and H.D. Ortiz: methodology and writing.

REFERENCES

Albuquerque Seismological Laboratory (ASL)/USGS, 1988. Global Seismograph Network - IRIS/USGS [Data set]. International Federation of Digital Seismograph Networks, doi:10.7914/SN/IU.

Albuquerque Seismological Laboratory (ASL)/USGS, 1992. New China Digital Seismograph Network [Data set]. International Federation of Digital Seismograph Networks, doi:10.7914/SN/IC.

Albuquerque Seismological Laboratory (ASL)/USGS, 2006. Caribbean USGS Network [Data set]. International Federation of Digital Seismograph Networks, doi:10.7914/SN/CU.

Ammon, C. J., Lay, T., Kanamori, H. & Cleveland, M., 2011. A rupture model of the 2011 off the Pacific coast of Tohoku Earthquake, *Earth, Planets Space,* **63**(33), 693–696.

Anthony., R. E., Watzak, J., Ringler, A. T. & Wilson, D. C., 2022. The nature and precision of direct acoustic-to-seismic coupling from local explosions, *Geophys. J. Int.,* **230,** 2019–2035.

Beauduin, R., Lognonné, P., Montagner, J. - P., Cacho, S., Karczewski, J. F. & Morand, M., 1996. The effects of atmospheric pressure changes on seismic signals or how to improve the quality of a station, *Bull. seism. Soc. Am.,* **86**(6), 1760–1769.

Bishop, J. W., Fee, D., Modrak, R., Tape, C. & Kim, K., 2021. Spectral element modeling of acoustic to seismic coupling over topography, *J. geophys. Res.,* **127**(1), e2021JB023142,.

Bormann, P., ed. 2012. *New Manual of Seismological Observatory Practice (NMSOP-2), IASPEI,* Deutsches GeoForschungszentrum GFZ, doi:10.2312/GFZ.NMSOP-2.

Carr, J. L., Horáth, A., Wu, D. L. & Friberg, M. D., 2022. Stereo plume height and motion retrievals for the record-setting Hunga Tonga-Hunga Ha'apai Eruption of 15 January, 2022, *Geophys. Res. Lett.,* **49,** e2022GL098131, doi:10.1029/2022GL098131.

Dahlen, F. A., 1982. The effect of data windows on the estimation of free oscillation parameters, *Geophys. J. Int.,* **69**(2), 537–549.

Dahlen, F. A. & Tromp, J., 1998. *Theoretical Global Seismology,* Princeton Univ. Press, 1025pp.

Dziewonski, A. M. & Anderson, D. L., 1981. Preliminary reference Earth model, *Phys. Earth planet. Inter.,* **25**(4), 297–356.

Edwards, W. N., Eaton, D. W., McCausland, P. J., ReVelle, D. O. & Brown, P. G., 2007. Calibrating infrasonic to seismic coupling using the Stardust sample return capsule shockwave: implications for seismic observations of meteors, *J. geophys. Res.,* **112**(B10), doi:10.1029/2006JB004621.

Harris, C. R. *et al.*, 2020. Array programming with NumPy, *Nature,* **585,** 357–362.

Jones, R. M. & Georges, T. M., 1976. Infrasound from convective storms. III. Propagation to the ionosphere, *J. acoust. Soc. Am.,* **59**(4), 765–779.

Kanamori, H. & Mori, J., 1992. Harmonic excitation of the mantle Rayleigh waves by the 1991 eruption of Mount Pinatubo, Philippines, *Geophys. Res. Lett.,* **19**(7), 721–724.

Kanamori, H., Mori, J. & Harkrider, D. G., 1994. Excitation of atmospheric oscillations by volcanic eruptions, *J. geophys. Res.,* **99**(B11), 21947–21961.

Kim, K., Lees, J. M. & Ruiz, M., 2012. Acoustic multipole source model for volcanic explosions and inversions for source parameters, *Geophys. J. Int.,* **191**(3), 1192–1204.

Lekić, V., Panning, M. & Romanowicz, B., 2010. A simple method for improving crustal corrections in waveform tomography, *Geophys. J. Int.,* **182**(1), 265–278.

Lognonné, P., Clévédé, E. & Kanamori, H., 1998. Computation of seismograms and atmospheric oscillations by normal-model summation for a spherical earth model with realistic atmosphere, *Geophys. J. Int.,* **135**(2), 388–406.

Masters, G., Barmine, M. & Kientz, S., 2014. Mineos user manual version 1.0.2, 99 pp., Available at: https://geodynamics.org/cig/software/mineos/mineos-manual.pdf, last accessed: February 2022.

Masters, G., Park, J. & Filbert, F., 1983. Observations of coupled spheroidal and toroidal modes, *J. geophys. Res.,* **88**(B12), 10 285–10 298.

Masters, G., Jordan, T. H., Silver, P. G. & Gilbert, F., 1982. Aspherical Earth structure from fundamental spheroidal-mode data, *Nature,* **298,** 609–613.

Matoza, R. S., Arciniega-Ceballos, A., Sanderson, R. W., Mendo-Pérez, G., Rosado-Fuentes, A. & Chouet, B. A., 2019. High-broadband seismoacoustic signature of Vulcanian explosions at Popocatépetl volcano, Mexico, *Geophys. Res. Lett.,* **46**(1), 148–157.

Matoza, R. S., Fee, D. & López, T. M., 2014. Acoustic characterization of explosion complexity at Sakurajima, Karymsky, and Tungurahua volcanoes, *Seismol. Res. Lett.,* **85**(6), 1187–1199.

Matoza, R. S. *et al.*, 2022. Atmospheric waves and global seismoacoustic observations of the January 2022 Hunga eruption, Tonga, *Science,* **377,** 95–100.

Megies, T., Beyreuther, M., Barsch, R., Krischer, L. & Wassermann, J., 2011. ObsPy – What can it do for data centers and observatories?, *Ann. Geophys.,* **54,** 47–58.

Met Office, 2015. Cartopy: a cartographic Python library with a Matplotlib interface, Exter, Devon, https://scitools.org.uk/cartopy, DOI:10.5281/zenodo.1182735.

Montagner, J.-P. & Kennett, B. L. N., 1996. How to reconcile body-wave and normal mode reference Earth models, *Geophys. J. Int.,* **125**(1), 229–248.

NASA, 2022. Tonga volcano plume reached the mesosphere, NASA Earth Observatory, Available at: https://earthobservatory.nasa.gov/images/149474/tonga-volcano-plume-reached-the-mesosphere, last accessed March 2022.

Newhall, C. G. & Self, S., 1982. The volcanic explosivity index (VEI) an estimate of explosive magnitude for historical volcanism, *J. geophys. Res.,* **82**(C2), 1231–1238.

Nishida, K., 2013. Earth's background free oscillations, *Annu. Rev. Earth planet. Sci.,* **41,** 719–740.

Pallister, J. S., Hoblitt, R. P. & Reyes, A. G., 1992. A basalt trigger for the 1991 eruptions of Pinatubo volcano?, *Nature,* **356,** 426–428.

Poli, P. & Shapiro, N. M., 2022. Rapid characterization of large volcanic eruptions: measuring the impulse of the Hunga Tonga explosion from teleseismic waves, **49**(8),.

Ringler, A. T. *et al.*, 2022. Achievements and prospects of global broadband seismic networks after 30 years of continuous geophysical observations, in press, doi:10.1029/2021RG000749.

Sailor, R. V. & Dziewonski, A. M., 1978. Measurements and interpretation of normal mode attenuation, *Geophys. J. Int.,* **53**(3), 559–581.

Schneider, S. & Deuss, A., 2021. A new catalogue of toroidal-mode overtone splitting function measurements, *Geophys. J. Int.,* **225**(1), 329–341.

Tahira, M., 1995. Acoustic resonance of the atmosphere at 3.7 mHz, *J. Atmos. Sci.,* **52**(15), 2670–2674.

Talavera-Soza, S. & Deuss, A., 2020. New measurements of long-period radial modes using large earthquakes, *Geophys. J. Int.,* **224**(2), 1211–1224.

Scripps Institution of Oceanography, 1986. IRIS/IDA Seismic Network, International Federation of Digital Seismograph Networks, doi:10.7914/SN/II.

Thiéry, R. & Mercury, L., 2009. Explosive properties of water in volcanic and hydrothermal systems, *J. geophys. Res.,* **114**(B5), doi:10.1029/2008JB005742.

Watada, S. & Kanamori, H., 2010. Acoustic resonant oscillations between the atmosphere and the solid earth during the 1991 Mt. Pinatubo eruption, *J. geophys. Res.,* **115**(B12), doi:10.1029/2010JB007747.

Widmer, R. & Zürn, W., 1992. Bichromatic excitation of long-period Rayleigh and air waves by the Mount Pinatubo and El Chichon volcanic eruptions, *Geophys. Res. Lett.,* **19**(8), 765–768.

Witze, A., 2022. Why the Tongan eruption will go down in the history of volcanology, *Nature,* **602,** 376–378.

Yuen, A. D. *et al.*, 2022. Under the surface: pressure-induced planetary-scale waves, volcanic lightning, and gaseous clouds caused by the submarine eruption of Hunga Tonga-Hunga Ha'apai volcano, *Earthq. Res. Adv.,* **2,** doi:10.1016/j.eqrea.2022.100134.

Zürn, W. & Meurers, B., 2009. Clear evidence for the sign-reversal of the pressure admittance of gravity near 3 mHz, *J. Geodyn.,* **48,** 371–377.

Zürn, W. & Widmer, R., 1995. On noise reduction in vertical seismic records below 2 mHz using local barometric pressure, *Geophys. Res. Lett.,* **22**(24), 3537–3540.

Zürn, W. & Widmer, R., 1996. World wide observations of bichromatic long-period Rayleigh-waves excited during the June 15, 1991 eruption of Mt. Pinatubo, in *Fire and Mud, Eruptions of Mount Pinatubo, Phillipines,* pp. 615–624, eds Newhall, C. & Punongbayan, J.R., Phillipine Institute of Volcanology and Seismology, Quezo City and University of Washington Press.

Zürn, W. & Wielandt, E., 2007. On the minimum of vertical seismic noise near 3 mHz, *Geophys. J. Int.,* **168**(2), 647–658.

SUPPORTING INFORMATION

Supplementary data are available at *GJI* online.

Figure S1. (a) Maximum amplitudes of spectra as a function of the antipodes of the great circle through the station and Honga Tonga eruption in the 3.5–3.8 mHz band for 12 hr data starting at 04:14:00 15 January 2022, UTC for all primary (location code 00) seismometers (channel code LHZ) across the Global Seismographic Network. Stations with signal-to-noise ratio (SNR) greater than 3 are denoted by circles, and stations with an SNR less than 3 are denoted by squares. The location of the Hunga Tonga eruption is denoted by a red star, and the antipode is depicted by a black star. (b) Same as (a), but for the frequency where the peak amplitude occurred.

Figure S2. Quality factor estimate (Q) for the vertical-component (channel LHZ) of Caribbean USGS Network (network code CU) station BBGH (Gun Hill, Barbados). We estimate the decay of the amplitudes in the 3.65–3.78 mHz band using 15-hr time windows starting on 15 January 2022, at 04:14:00 UTC. Our estimate of $Q = 334$ is obtained by fitting a slope (orange), in the least-squares sense, to the average power estimate in each time window in nm s^{-2} (blue). For reference we include $Q = 191$ for 0S29 from PREM (Dziewonski & Anderson 1981) in green after scaling by the mean of our measurements.

Figure S3. Estimates of Q in the 3.65–3.78 mHz band at GSN stations using 30 hr data with a window of 15 hr. Stations with a relative residual of less than one are plotted as circles, while all others are plotted with squares. The location of the Hunga Tonga eruption is denoted by a red star, and the antipode is depicted by a black star.

Figure S4. Estimates of Q in the 3.65–3.78 mHz band at the antipodes of the great circle between GSN stations and the Hunga Tonga eruption using 30 hr of data with a window of 15 hr. Stations with a relative residual of less than one are plotted as circles, while all others are plotted with squares. The location of the Hunga Tonga eruption is denoted by a red star, and the antipode is depicted by a black star.

Figure S5. (a) 26 hr of time-series of pressure data from the Australian Government Bureau of Meteorology (AGBOM) barometer located in Samoa (latitude 13.8267, longitude −171.7611, orange) starting at 04:14:00 15 January 2022, UTC as well as for the IRIS/USGS station AFI (Afiamalu, Samoa). (b) Corresponding spectra from the time-series in (a). For reference, we include the frequencies of 0S28 (3.63 mHz, red) and 0S29 (3.72 mHz, purple) as estimated by the preliminary reference Earth model (PREM; Dziewonski & Anderson 1981) as well as the atmospheric modes ${}_0S_{28}$–${}_0S_{29}$ (3.68 mHz, orange) and ${}_0S_{36}$–${}_0S_{37}$ (4.40 mHz, green) from Lognonné *et al.* (1998).

Figure S6. Pressure spectra from 26 hr of data starting at 04:14:00 15 January 2022, UTC for all microbarographs (channel code LDO or LDI) across the Global Seismographic Network (blue). For reference we include the frequencies of 0S28 (3.63 mHz, red) and 0S29 (3.72 mHz, purple) as estimated by the Preliminary Reference Earth Model (PREM; Dziewonski & Anderson 1981) as well as the atmospheric modes ${}_0S_{28}$–${}_0S_{29}$ (3.68 mHz, orange) and ${}_0S_{36}$–${}_0S_{37}$ (4.40 mHz, green) from Lognonné *et al.* (1998). Stations CMLA, PALK, PTCN, OBN and SFJD are not shown as they displayed obvious instrumental problems in the records. For BFO we are using the 10 location code LDO pressure record.

Figure S7. Estimates of Q in the 3.65–3.78 mHz band at GSN stations using 30 hr of data with a window of 15 hr following the 1991 Pinatubo event. Stations with a relative residual of less than one are plotted as circles, while all others are plotted with squares.

Please note: Oxford University Press is not responsible for the content or functionality of any supporting materials supplied by the authors. Any queries (other than missing material) should be directed to the corresponding author for the paper.